

Unprecedented electrocatalytic oxygen evolution performances by cobalt-incorporated molybdenum carbide microflowers with controlled charge re-distribution

Md. Selim Arif Sher Shah¹, Vinod K. Paidi², Hyeonjung Jung³, Sungsoon Kim¹, Geunsik Lee⁴, Jeong Woo Han^{3,5,*}, Kug-Seung Lee^{2,*}, and Jong Hyeok Park^{1,*}

¹Department of Chemical and Biomolecular Engineering, Yonsei University, 50 Yonsei-ro, Seodaemun-gu, Seoul 03722, Republic of Korea, E-mail: lutts@yonsei.ac.kr

²Beamline Division, Pohang Accelerator Laboratory, 80 Jigok-ro 127 beon-gil, Pohang, 37673 Gyeongbuk, Republic of Korea, E-mail: lks3006@postech.ac.kr

³Department of Chemical Engineering, Pohang University of Science and Technology, Pohang 37673, Republic of Korea, E-mail: jwhan@postech.ac.kr

⁴Department of Chemistry, Ulsan National Institute of Science and Technology (UNIST), 50 UNIST-gil, Ulsan 44919, Republic of Korea

⁵Institute for Convergence Research and Education in Advanced Technology, Yonsei University, 50 Yonsei-ro, Seodaemun-gu, Seoul 03722, Republic of Korea

M. S. A. Sher Shah, V. K. Paidi and H. Jung contributed equally to this work

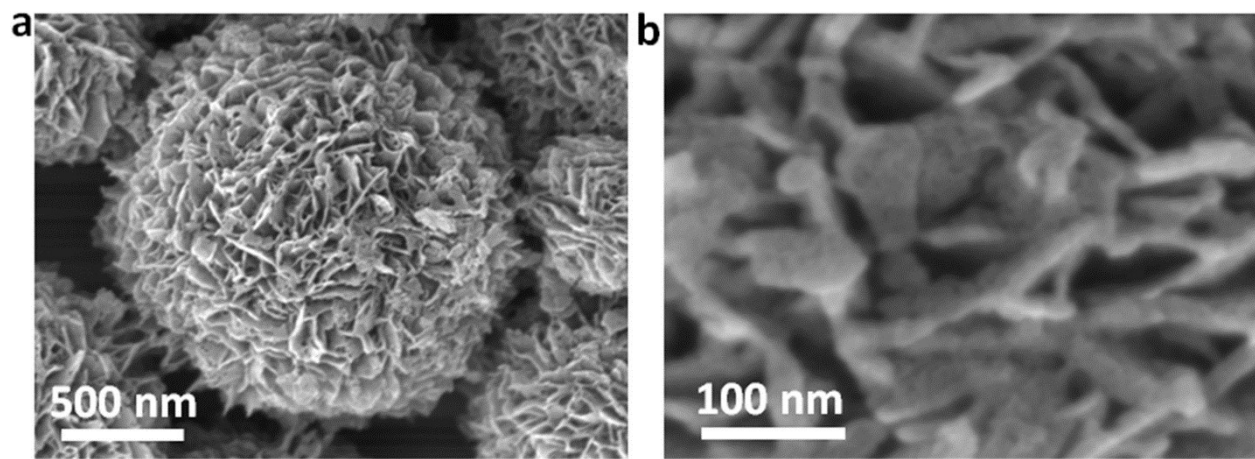


Fig. S1 SEM micrographs of the Mo-PDA microflowers at different magnifications.

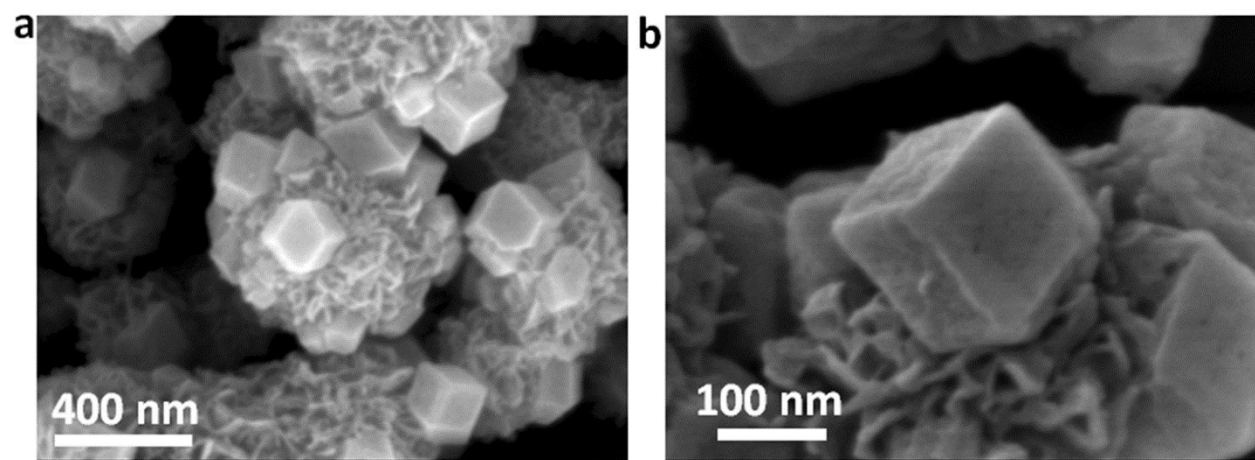


Fig. S2 SEM micrographs of the ZIF-67@Mo-PDA microflowers at different magnifications.

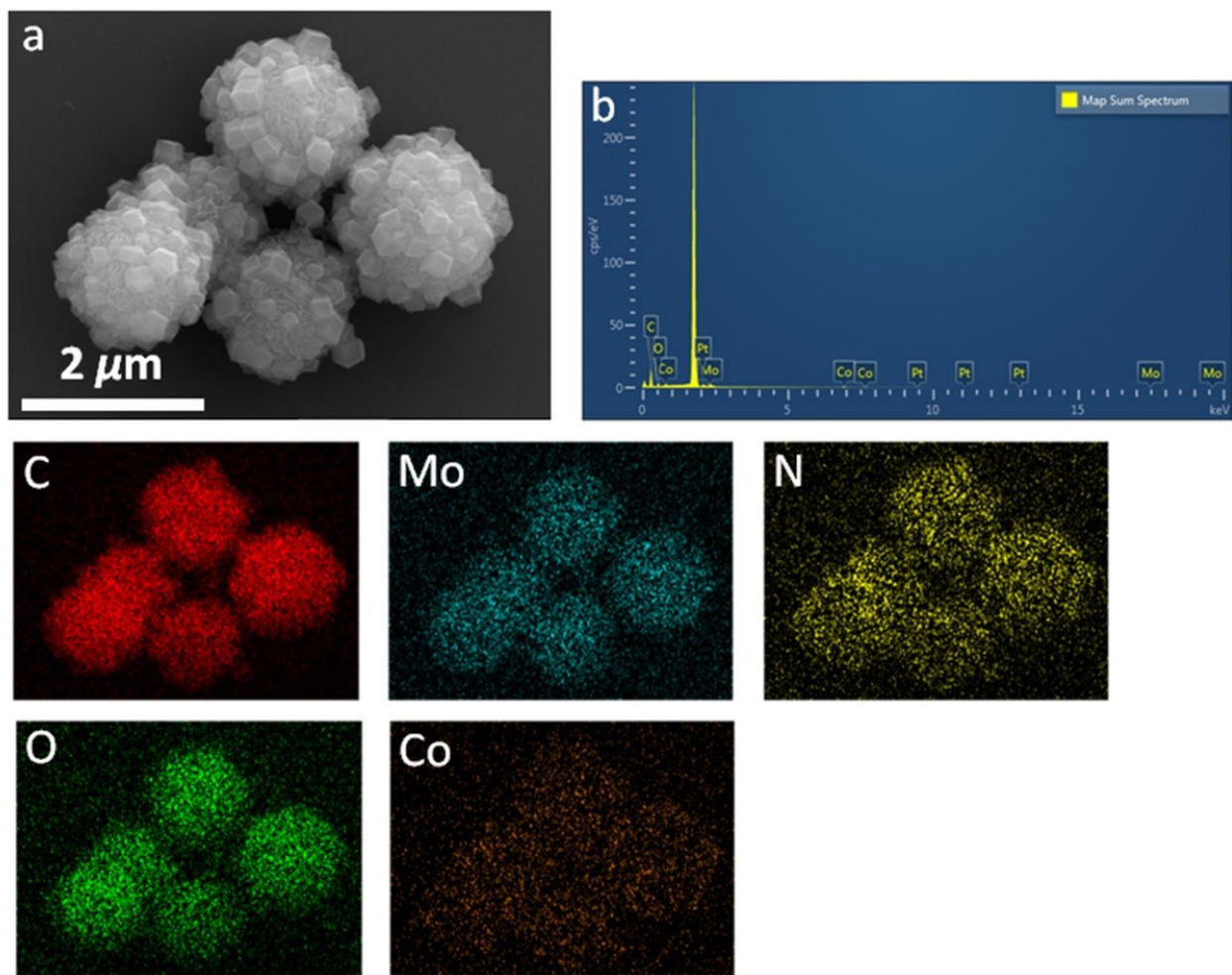


Fig. S3 (a) FESEM micrograph, (b) EDX spectrum and elemental mapping of 3D ZIF-67-1.5@Mo-PDA microflowers showing the presence of Mo, Co, C, N and O.

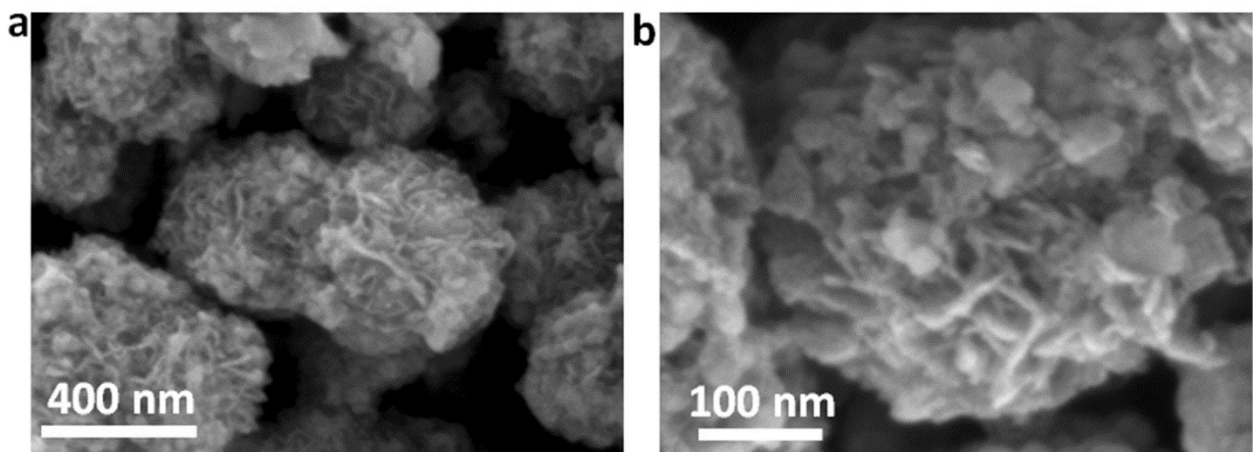


Fig. S4 SEM micrographs of the MoCo1.5C-700 microflowers at different magnifications.

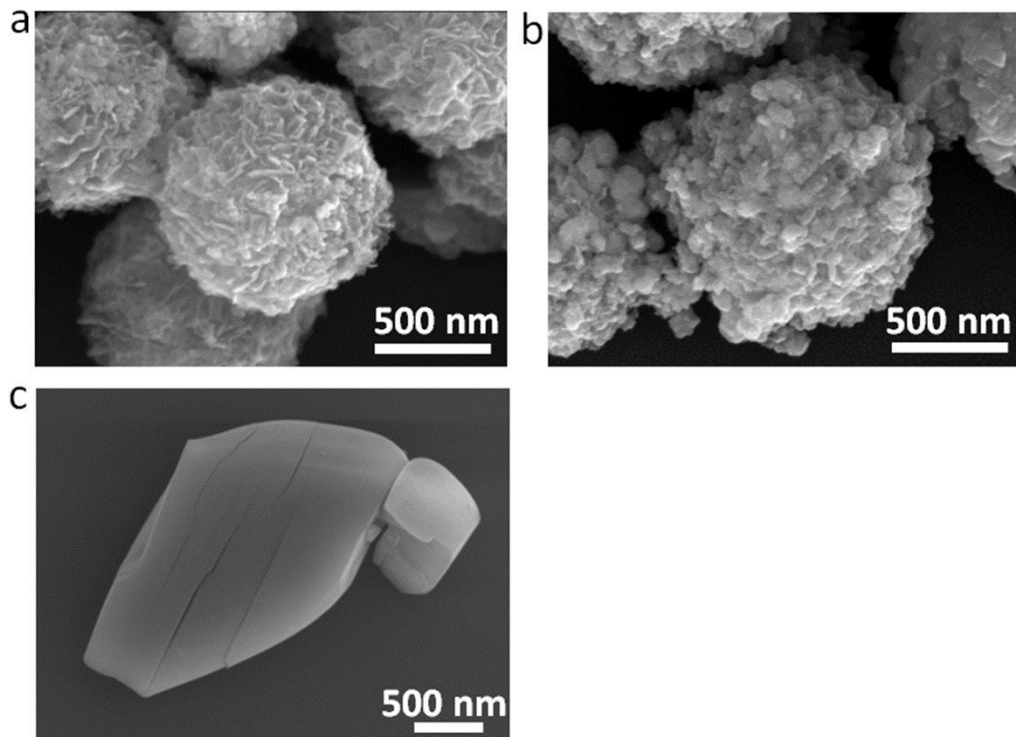


Fig. S5 SEM micrographs of the MoCo1.5C-600 microflowers (a), MoCo1.5C-800 microflowers (b) and MoCo1.5C-900 (c).

Table S1 Data obtained from the Rietveld refinements of MoCo1.5C-700 microflowers.

Phase	Space group	Lattice constant (Å)	Crystallite size (nm)	Phase fraction (%)
Mo ₃ Co ₃ C	Fd-3m	a=11.031±0.001 b=11.031±0.001 c=11.031±0.001	22.8±0.2	53±2
MoC	Fm-3m	a=4.247±0.001 b=4.247±0.001 c=4.247±0.001	5.4±0.1	30±2
MoO ₂	P21/c	a=5.519±0.001 b=4.840±0.001	7.5±0.1	17±1

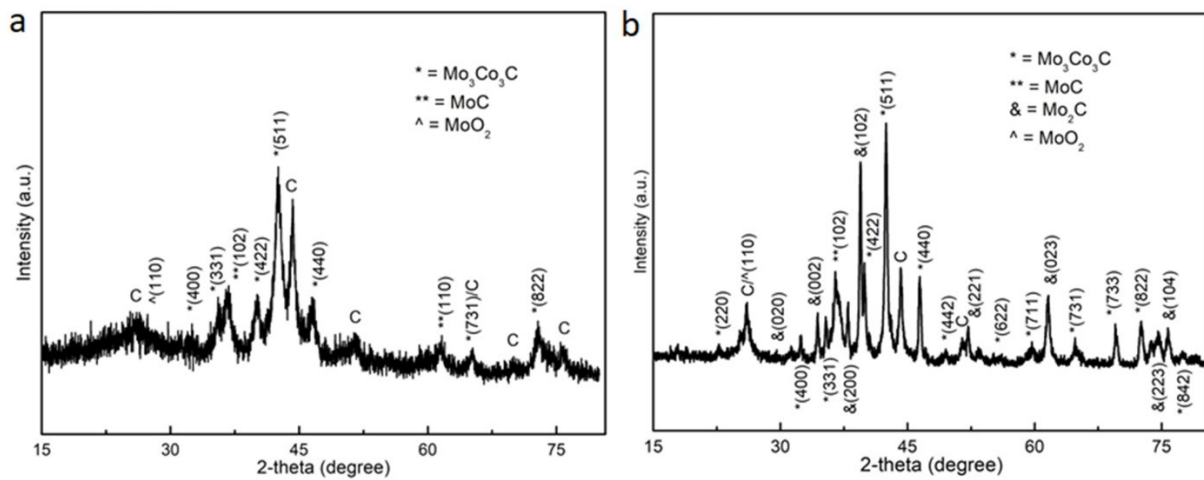


Fig. S6 XRD pattern of MoCo1.5C-600 microflowers (a) and MoCo1.5C-800 microflowers (b).

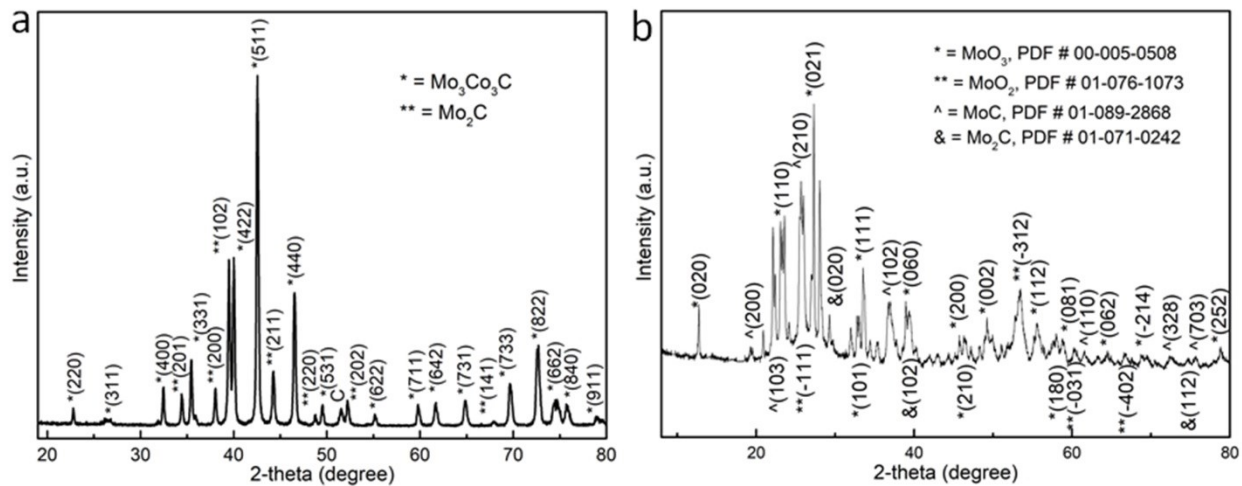


Fig. S7 XRD pattern of (a) MoCoC-750 and (b) Mo-PDA derived Mo₂C.

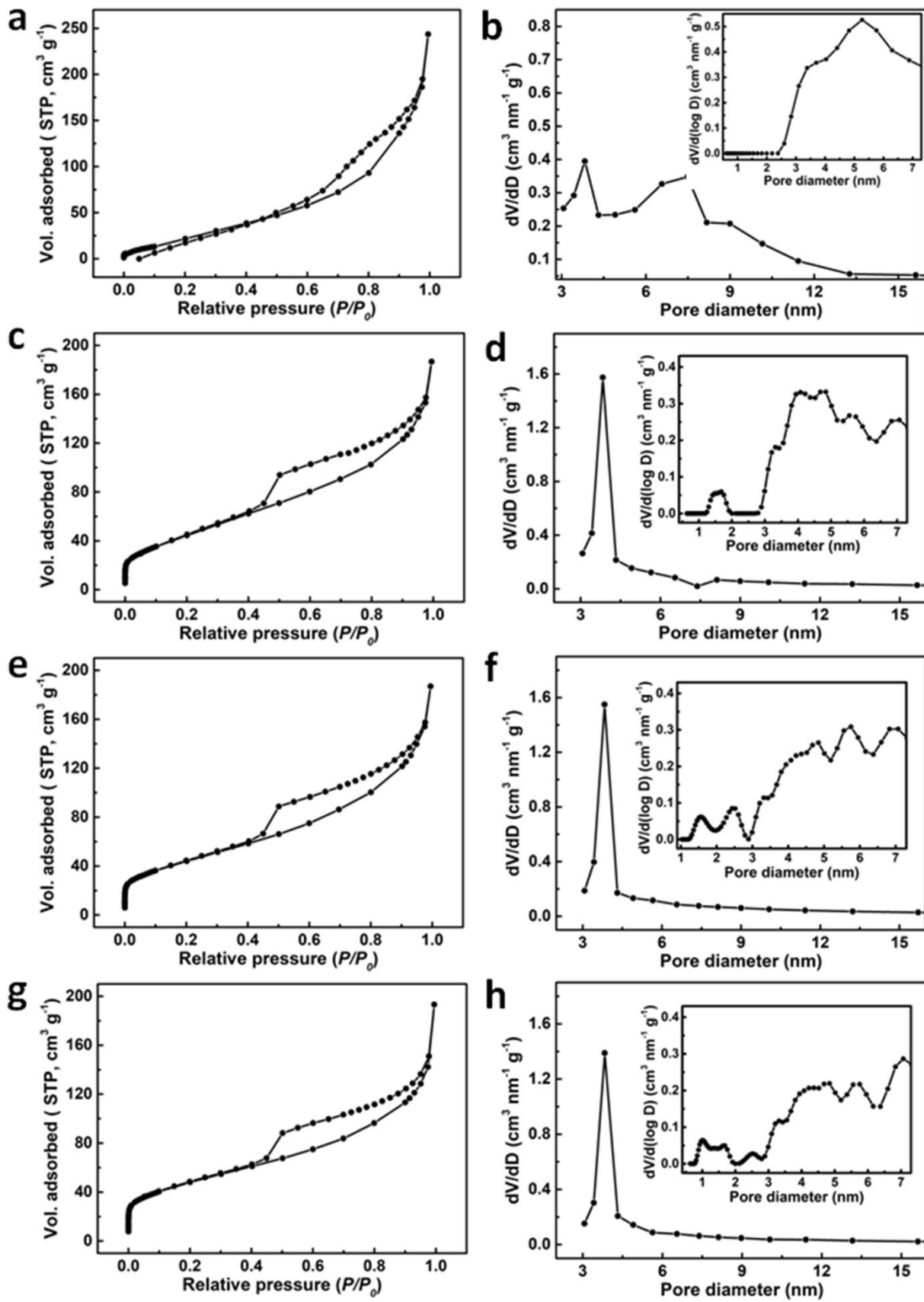


Fig. S8 Nitrogen sorption data for (a) MoCo0.5C-700, (c) MoCo1.0C-700, (e) MoCo1.5C-700 and (g) MoCo2.0C-700 microflowers. The corresponding pore size distribution plots are shown in panels (b), (d), (f) and (h). The insets in b, d, f and h are the DFT pore size distribution curves.

Table S2 Nitrogen sorption data of the different samples.

Sample	BET surface area (m ² g ⁻¹)	Pore size (nm)	Pore volume (cm ³ g ⁻¹)
MoCo0.5C-700	65	3.83, 5.6	0.41
MoCo1.0C-700	161	3.83, 1.5, 1.7	0.27
MoCo1.5C-700	170	3.83, 1.6, 2.4	0.27
MoCo2.0C-700	174	3.83, 1.0, 1.7, 2.5	0.27

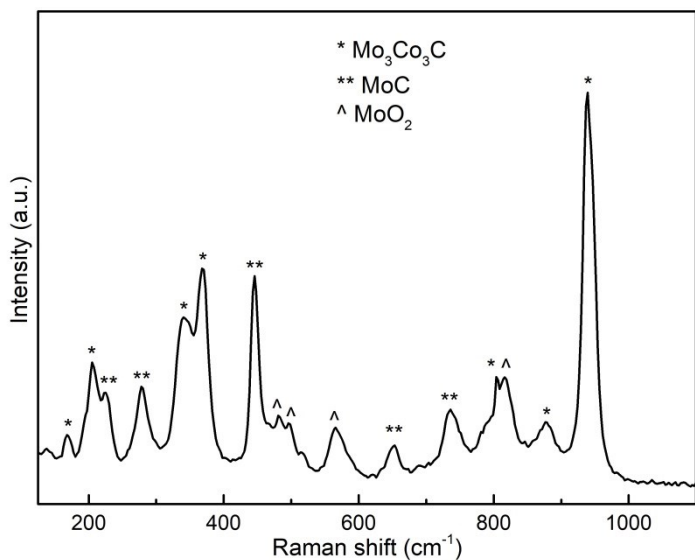


Fig. S9 Raman spectrum of MoCo1.5C-700 microflowers showing the presence of Mo₃Co₃C, Mo₂C and Co₂C.^{1–7}

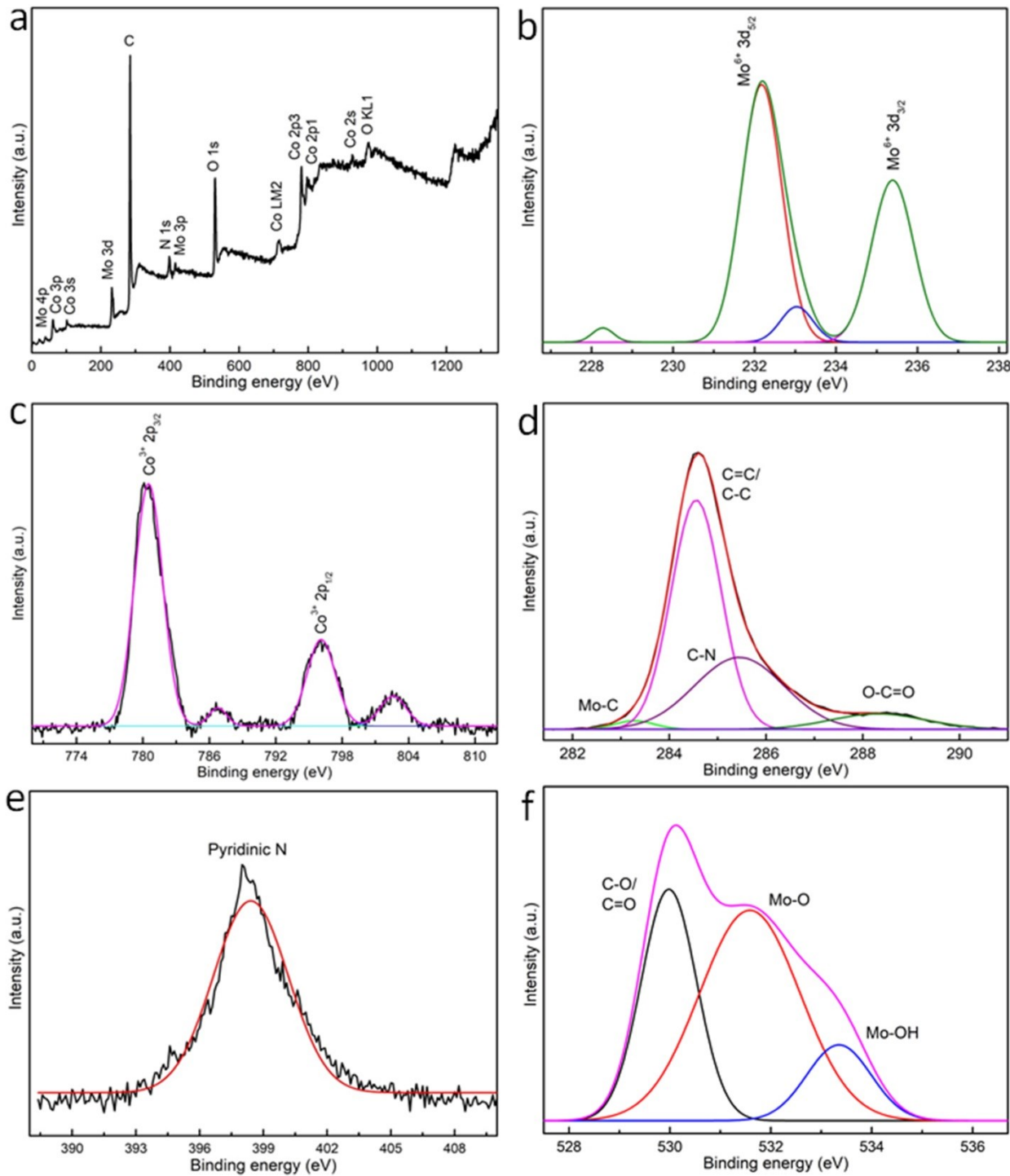


Fig. S10 The survey XPS spectrum (a) of the MoCo1.5C-700 microflowers shows the presence of Mo, Co, C, N and O. High resolution XPS spectrum of (b) Mo 3d, (c) Co 2p, (d) C 1s, (e) N 1s and (f) O 1s. N 1s core level XPS spectrum shows that N are pyridinic.

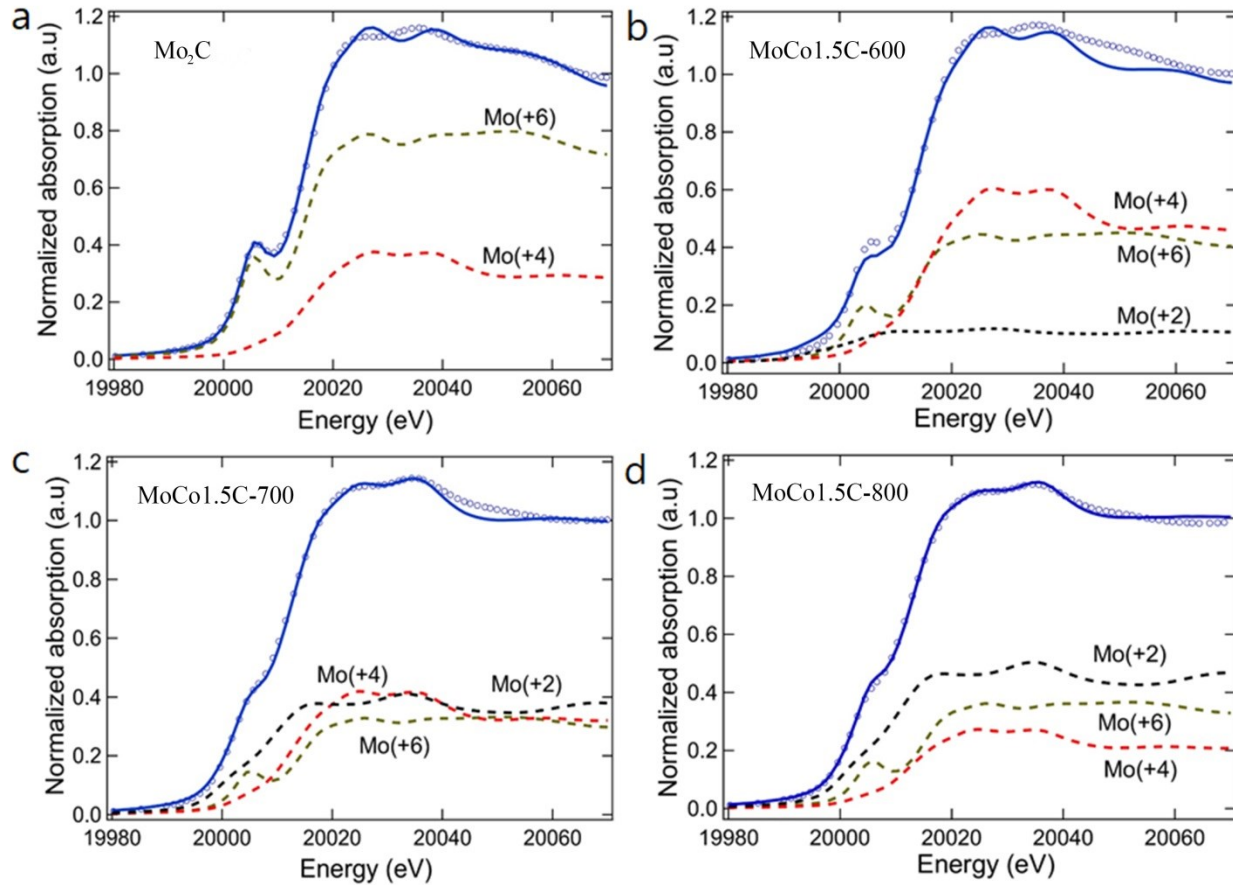


Fig. S11 The results of the LCF for the normalized Mo K-edge XANES spectra (open circles) and corresponding best fits (solid lines) are shown. The dashed lines are the measured standards for the Mo (+2), Mo (+4), and Mo (+6) oxidation states. The weighting factors of each fit were summed to 100%, as shown in the table below. The R-factor is defined as the normalized sum of the squared residuals of the fit and indicates the quality of the fit.

Table S3_A Linear combination fit results of Mo K-edge XANES.

Sample	Mo (+2)	Mo (+4)	Mo (+6)	R-factor
Mo ₂ C	--	44±2	52±4	0.004
MoCo1.5C-600	10±6	47±4	43±5	0.006
MoCo1.5C-700	36±5	33±2	31±5	0.002
MoCo1.5C-800	44±2	21±1	35±2	0.001

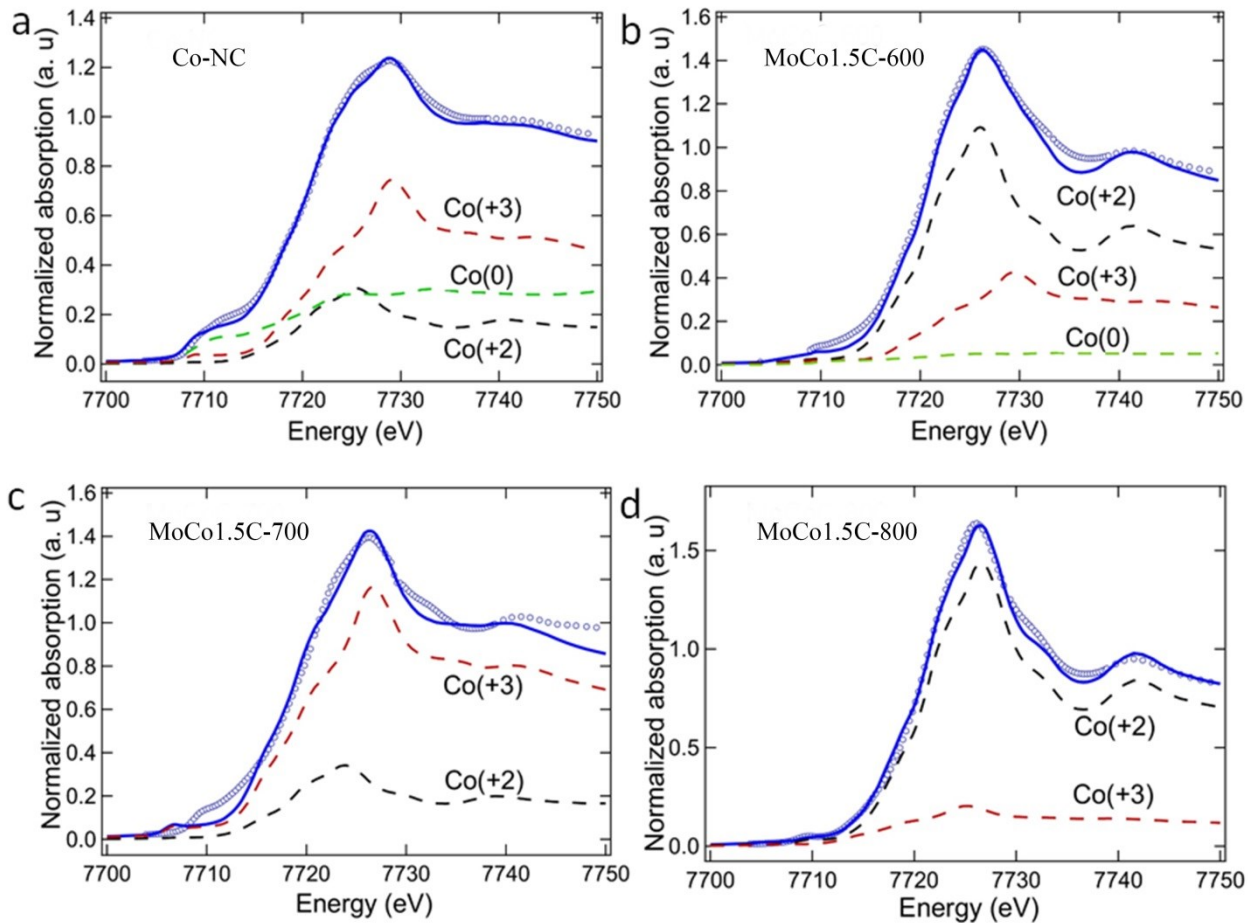


Fig. S12 The results of the LCF for the normalized Co K-edge XANES spectra (open circles) and corresponding best fits (solid lines) are shown. The dashed lines are the measured standards for Co (0), Co (+2), and Co (+3) oxidation states. The weighting factors of each fit were summed to 100%, as shown in the table below. The R-factor is defined as the normalized sum of the squared residuals of the fit and indicates the quality of the fit.

Table S3_B Linear combination fit results from Co K-edge XANES data.

Sample	Co (0)	Co (+2)	Co (+3)	R-factor
Co-NC	31±2	18±2	51±2	0.002
MoCo1.5C-600	6±2	65±1	29±2	0.008
MoCo1.5C-700	--	20±3	80±3	0.009
MoCo1.5C-800	--	86±2	14±4	0.003

Table S3_C EXAFS fit parameters of the samples. Here, N = coordination number, R = interatomic distance, σ^2 = Debye-Waller factor (bond disorder), R-Factor = a measure of the quality of EXAFS fit); ** Scattering paths obtained from the crystallographic phase.

Sample	Path	Source**	E_0 (eV)	N	R (Å)	σ^2 (Å)	R-factor
Mo ₂ C	Mo – O	MoO ₃		1	1.71(1)	0.001(1)	
	Mo – C	MoC	-4(4)	2	2.04(2)	0.001(1)	
	Mo – Mo	MoO ₂		1	2.55(3)	0.012(4)	0.01
MoCo1.5C-600	Mo – O	MoO ₃		1	1.73(1)	0.0008(6)	
	Mo – C	Mo ₃ Co ₃ C		2	2.09(1)	0.005(2)	
	Mo – Mo	MoO ₂	-6(2)	1	2.55(1)	0.009(3)	0.02
MoCo1.5C-700	Mo – C	Mo ₃ Co ₃ C		2	2.13(1)	0.003(1)	
	Mo – Co	Mo ₃ Co ₃ C		2	2.73(1)	0.003(1)	
				-1(2)			0.02
MoCo1.5C-800	Mo – C	Mo ₃ Co ₃ C		2	2.14(2)	0.003(1)	
	Mo – Co	Mo ₃ Co ₃ C		2	2.75(1)	0.003(1)	
				3(2)			0.02

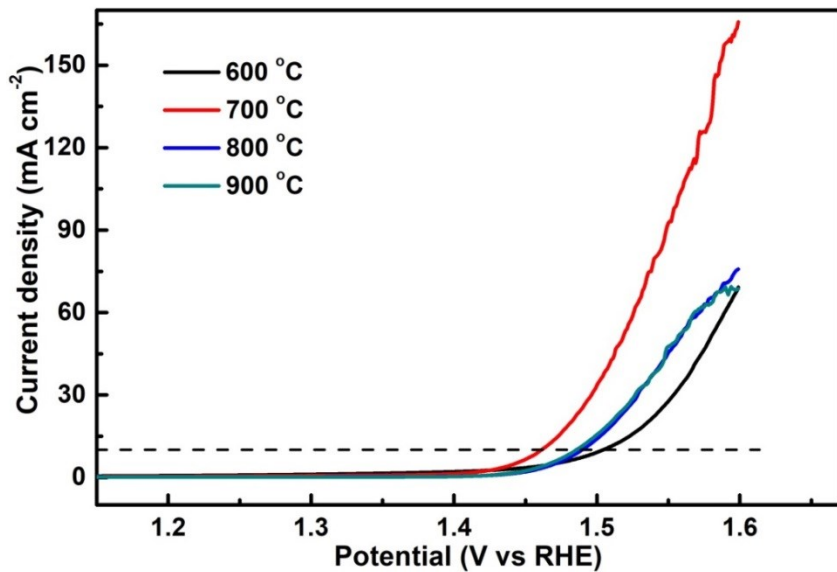


Fig. S13 OER performance of MoCo_{1.5}C-600/700/800 microflowers and MoCo_{1.5}C-900.

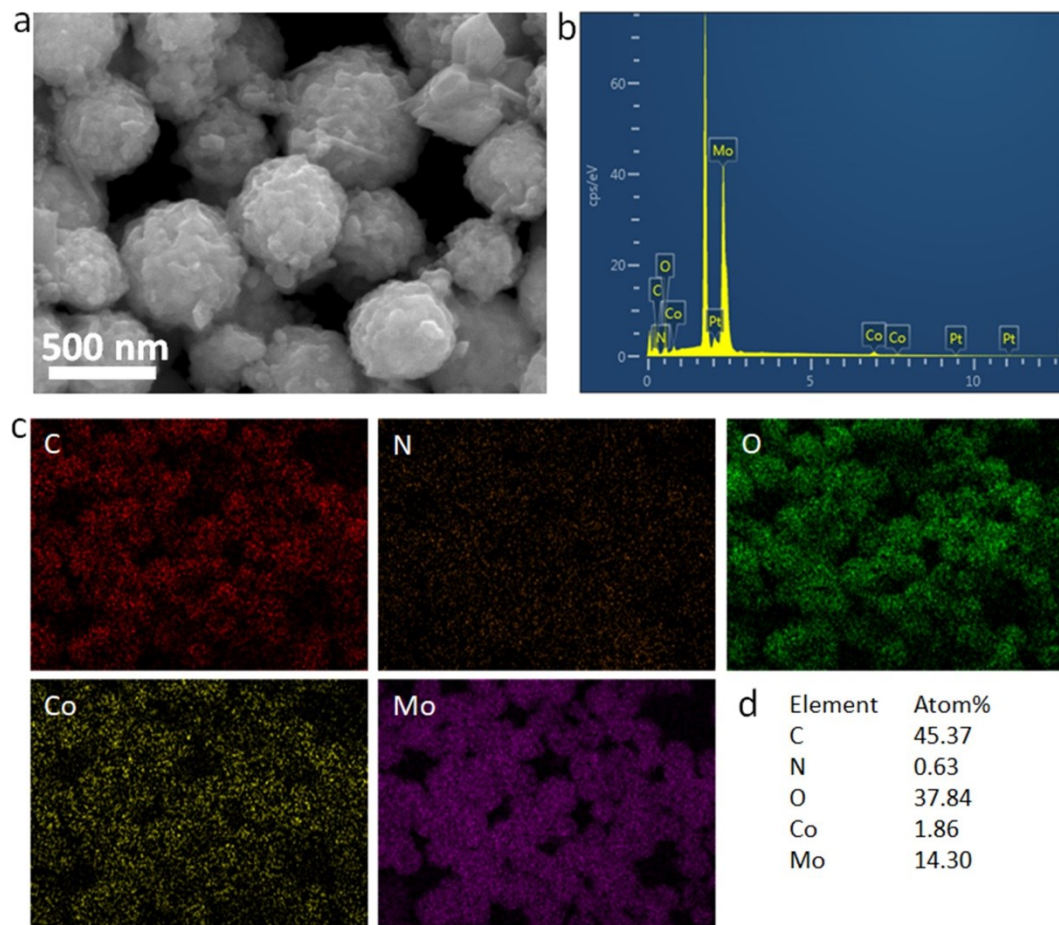


Fig. S14 (a) SEM, (b) EDX, (c) elemental mapping and (d) elemental composition of Co-Mo₂C.

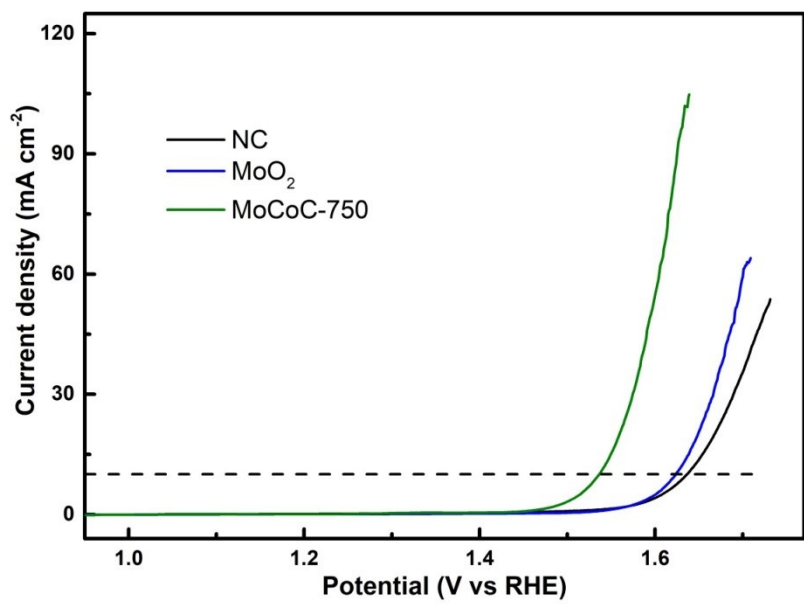
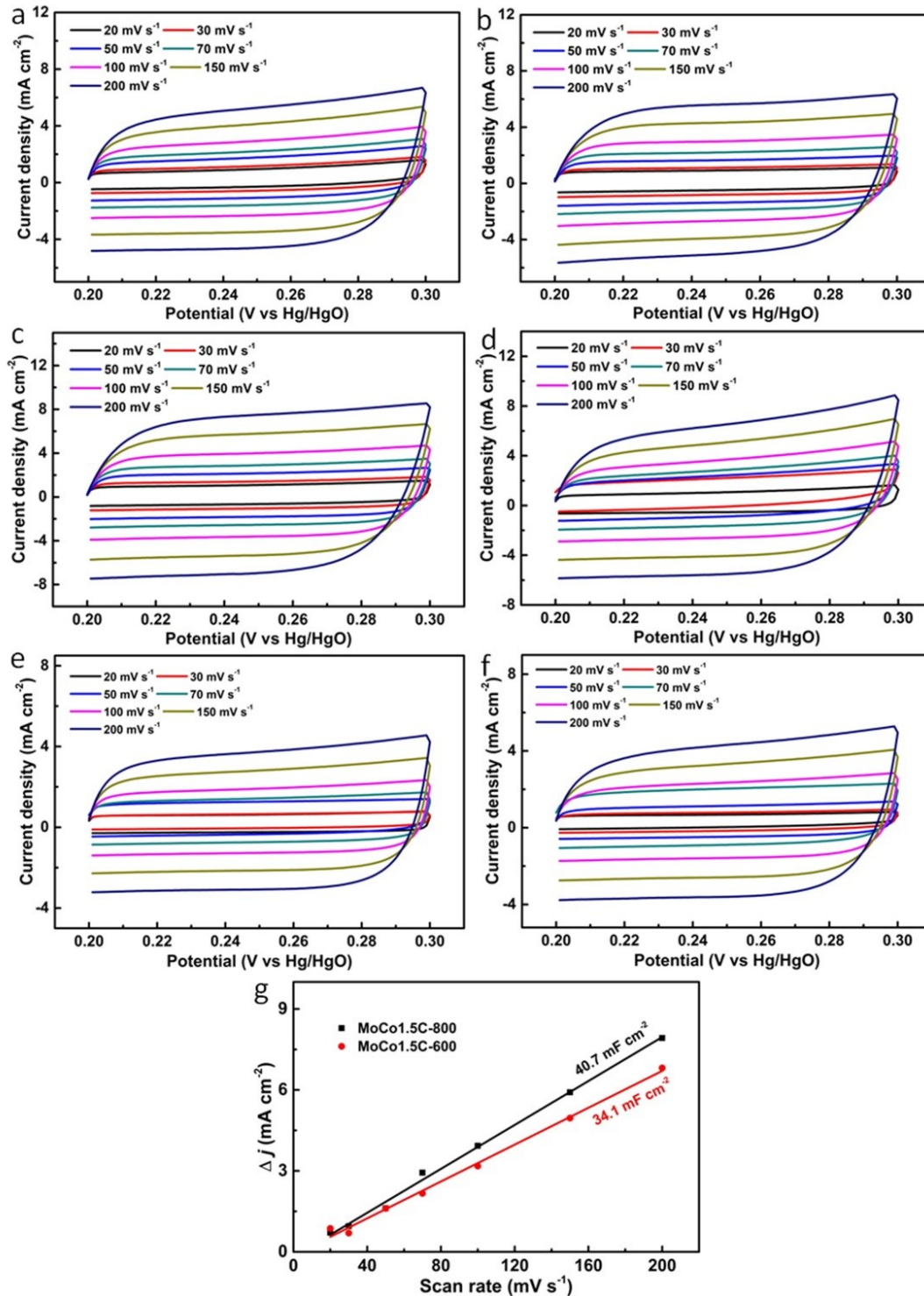


Fig. S15 OER performance of NC, MoO_2 and MoCoC-750.

Table S4 Comparison of the performance of the MoCo1.5C-700 microflowers electrocatalyst for oxygen evolution with the recent literature.

Electrocatalyst	Electrolyte	η_{10} (mV)	Tafel slope (mV dec ⁻¹)	Substrate	Ref
MoCo1.5C-700 microflowers	1.0 M KOH	232.5	61	GCE	This work
^a Co _{0.1} - β -Mo ₂ C@NC	1.0 M KOH	262.2	29	GCE (RDE)	⁸
Co ₄ Mo ₂ @NC	1.0 M KOH	330	46.1	GCE	⁹
B,N:Mo ₂ C@BCN NPs	1.0 M KOH	290	61	GCE	¹⁰
Ni-Mo _x C/NC-100	1.0 M KOH	328	74	GCE	¹¹
^b Zn _{0.35} Co _{0.65} O	1.0 M KOH	322	42.6	GCE (RRDE)	¹²
Co ₆ Mo ₆ C ₂ /NCRGO	1.0 M KOH	260	50	GCE	¹³
^c Fe-Co-P nanobox	1.0 M KOH	269	31	CFP	¹⁴
NiFe-LDH	1.0 M KOH	300	40	GCE (RDE)	¹⁵
Co-NC@Mo ₂ C	1.0 M KOH	347	61	GCE	¹⁶
NiCo-UMOFNs	1.0 M KOH	250	42	GCE	¹⁷
(Ni ₂ Co) _{0.925} Fe _{0.075} -MOF	1.0 M KOH	257	41.3	GCE	¹⁸
NiFe-UMNs	1.0 M KOH	260	30	GCE	¹⁹
Co-Mo ₂ C	0.1 M KOH	347	38	GCE (RDE)	²⁰
CoP/NCNHP	1.0 M KOH	310	70	GCE	²¹

^aRDE, ^bRRDE and ^cCFP are a rotating disk electrode, rotating ring disc electrode and carbon fiber paper, respectively.



Calculation of ECSA²²

Electrical double layer capacitance, $E_{dl} = \frac{1}{2} * \text{slope of current density vs scan rate plot.}$

$$\text{ECSA (cm}^2\text{)} = E_{dl}/60 \mu\text{F cm}^{-2}.$$

Table S5 Slope of potential vs difference in cathodic and anodic current density at 0.25 mV (vs Hg/HgO), specific capacitance and ECSA of different samples.

Sample	^a Slope ($m\text{F cm}^{-2}$)	E_{dl} ($m\text{F cm}^{-2}$)	ECSA (cm^2)
MoCo0.5C-700	47.9	23.95	399
MoCo1.0C-700	51.5	25.75	429
MoCo1.5C-700	70.8	35.4	590
MoCo2.0C-700	57.8	28.9	481
MoCo1.5C-600	34.1	17.0	284
MoCo1.5C-800	40.7	20.3	339

^aNormalized with respect to the geometrical surface area of the glassy carbon electrode.

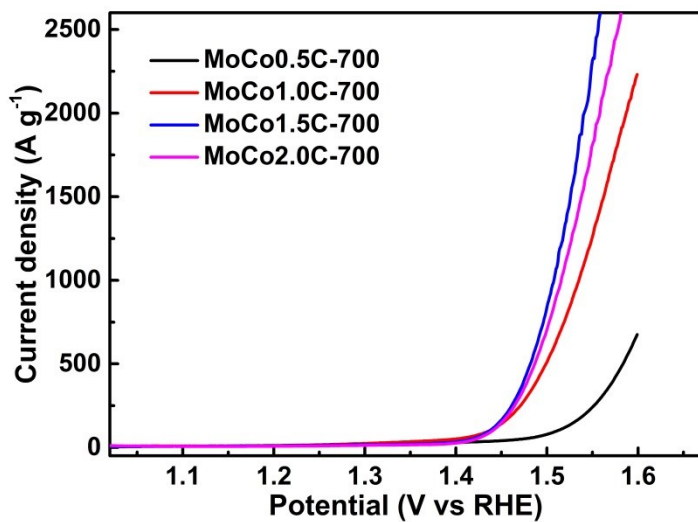


Fig. S17 Mass activity of different electrocatalysts.

We determined the k-point for the Brillouin Zone according to the literature [Sholl, David, and Janice A. Steckel. *Density functional theory: a practical introduction*. John Wiley & Sons, 2011.].

First, the k points of bulk models were tested based on the convergence criterion within 0.001 eV for total energies per atom. Figure S18 shows the calculated total energies per atom for Mo₂C and Mo₃Co₃C bulk models with increasing k points generated by the Monkhorst-Pack method. The energies were converged when the M is over 9 and 3 in bulk Mo₂C and Mo₃Co₃C calculations, respectively. In case of the a-axis and b-axis in the slab models, which define the surface plane, we referred to the fact that the reciprocal lattice vector is inversely proportional to the lattice parameter of the supercell. The k points for the two axes were determined by multiplying the converged k points of the bulk model by the ratio between the lattice parameters of bulk and slab models. Since the vacuum region in the slab model makes the electron density tail off to zero at the edge of the slab, using just one k point for the c-axis can make the accurate calculations possible. As a result, the $9 \times 9 \times 9$, $5 \times 5 \times 1$, $3 \times 3 \times 3$, and $3 \times 3 \times 1$ Monkhsor-Pack grid were selected for Mo₂C bulk, Mo₂C slab, Mo₃Co₃C bulk, and Mo₃Co₃C slab model calculations, respectively.

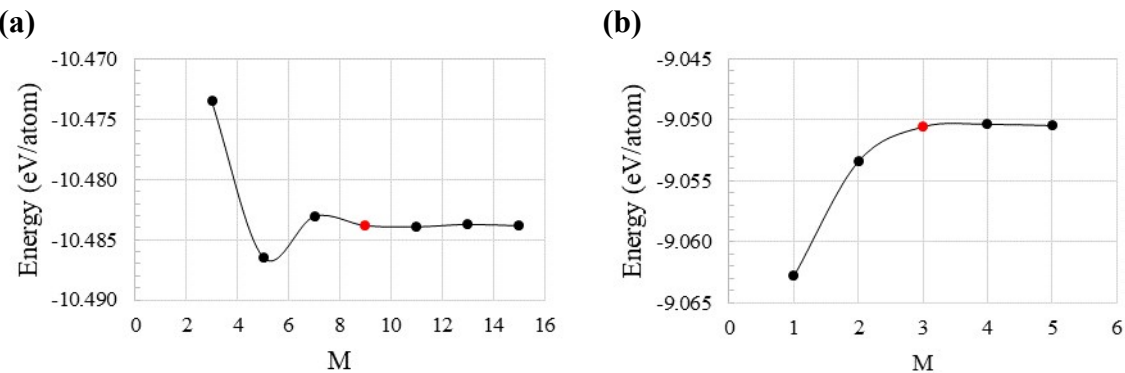


Fig. S18 Total energies per atom for bulk (a) Mo₂C and (b) Mo₃Co₃C with $M \times M \times M$ Monkhsor-Pack grid. Red dots denote the selected values.

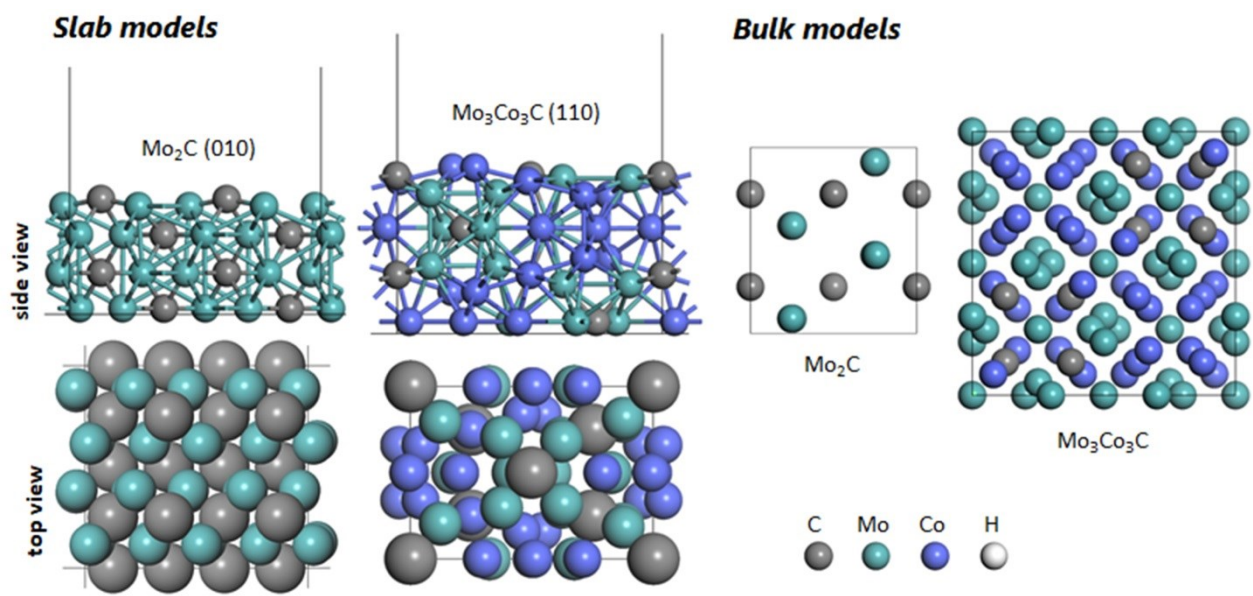


Fig. S19 Different models of Mo₂C (010) and Mo₃Co₃C (110) facet for the DFT calculation.

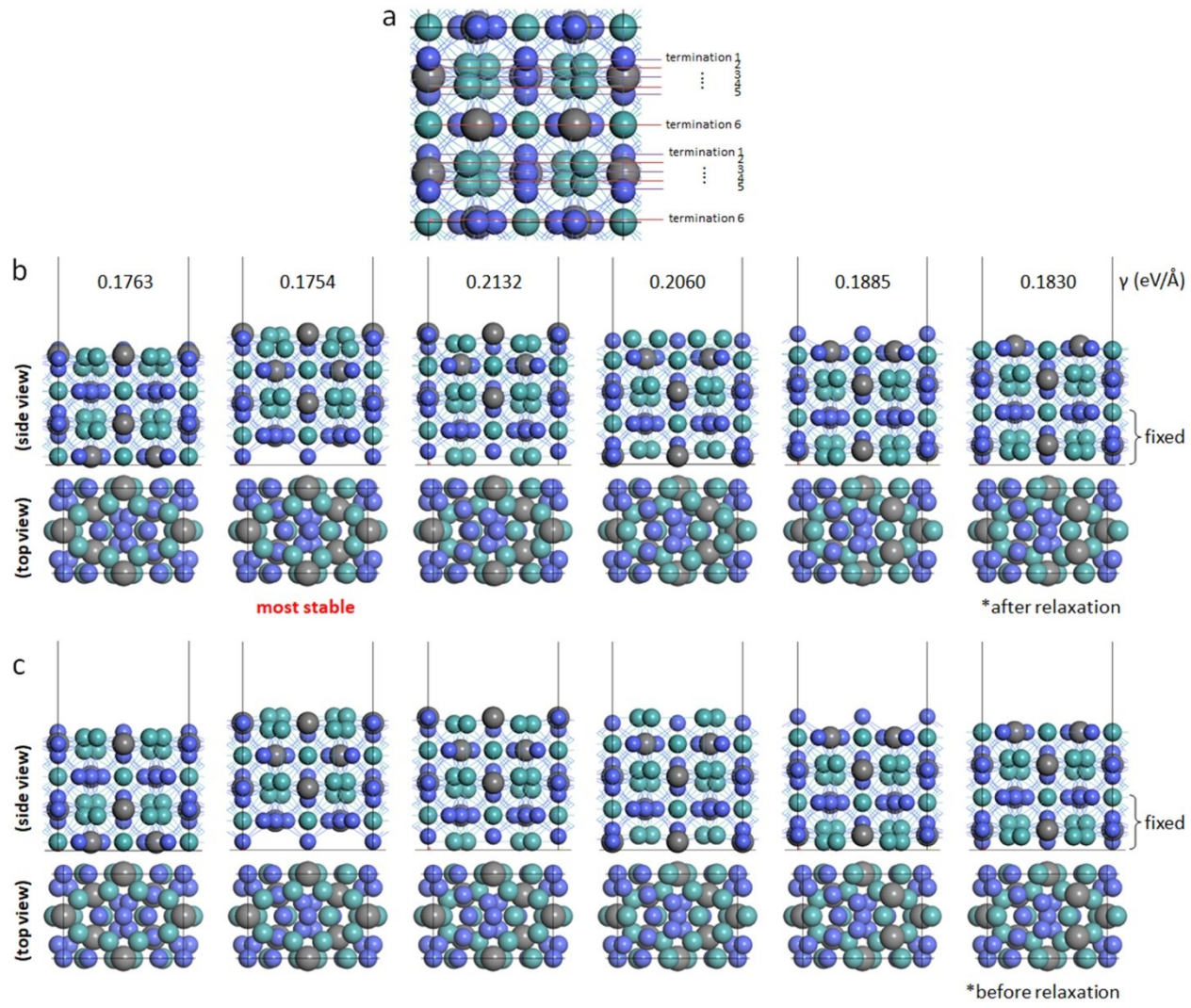


Fig. S20 (a) Different terminations of $\text{Mo}_3\text{Co}_3\text{C}$ (110) surface. (b) and (c) are the structures of various surface terminations and their energy.

Surface energy was calculated using the following equation.

$$\gamma = (E_{\text{slab}} - n \cdot E_{\text{bulk}})/A$$

where, γ : surface energy, E: DFT energy, n: stoichiometric parameter and A: surface area.

Table S6 Lattice constants (\AA) of Mo_2C and $\text{Mo}_3\text{Co}_3\text{C}$ for the DFT calculation and some references.

	a	b	c	
	4.738	6.060	5.232	This work
Mo_2C	4.738	6.038	5.210 ²³	
	4.741	6.070	5.227 ²⁴	
	4.732	6.037	5.199 ²⁵	
$\text{Mo}_3\text{Co}_3\text{C}$	11.05	11.05	11.05	This work
	11.07	11.07	11.07	Handbook of Inorganic Substances 2017.

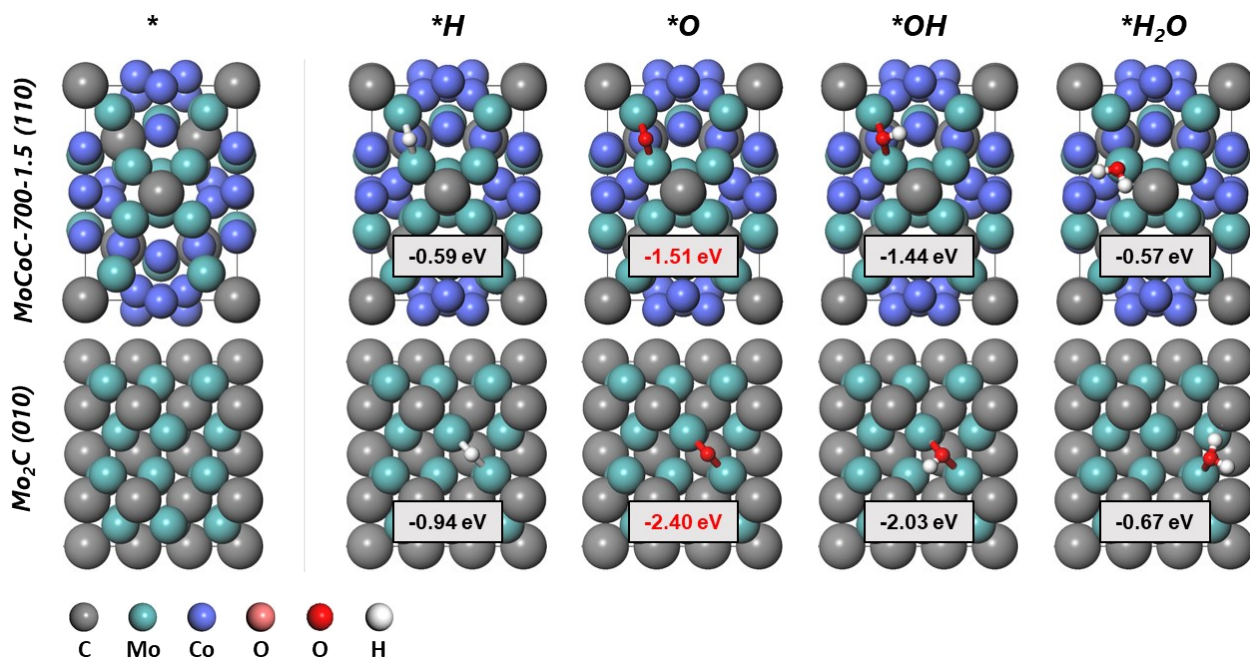
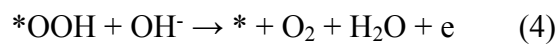
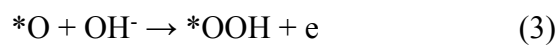
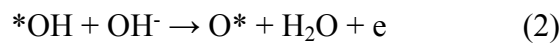
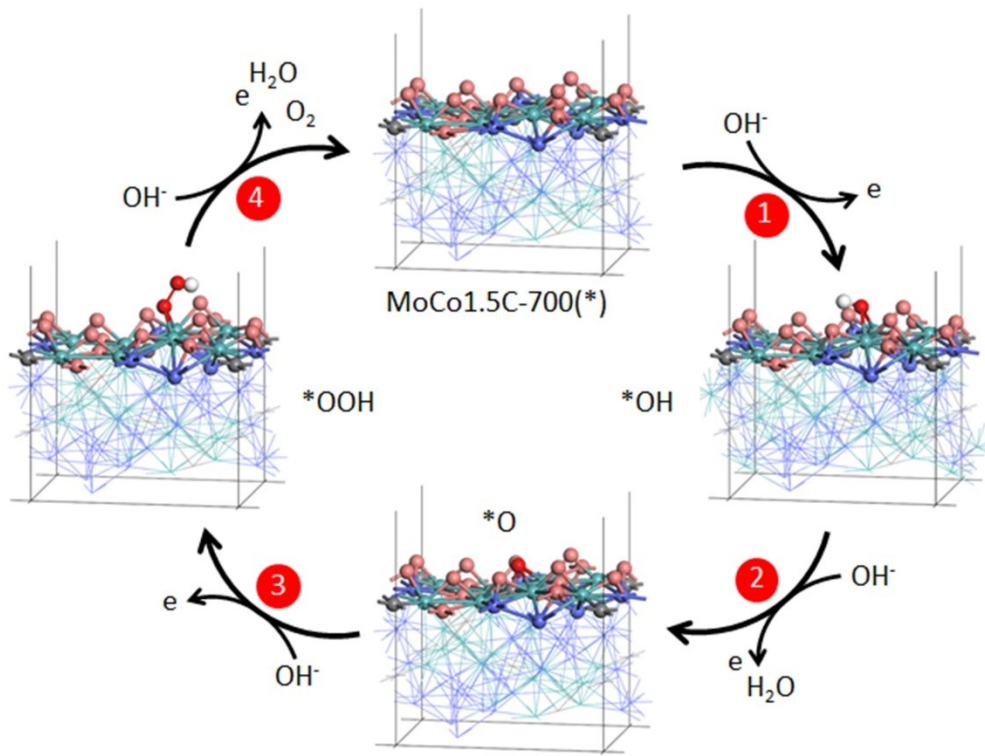
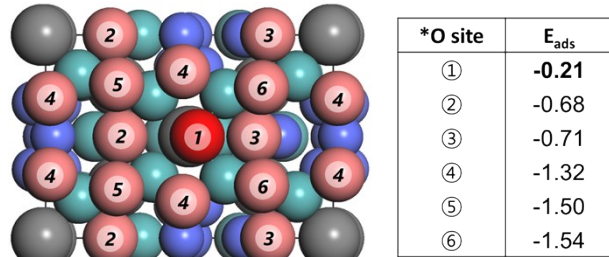


Fig. S21 The structure and binding energies (the insets) of water-induced adsorbents (H, O, OH and H_2O) on bare Mo_2C (010) and MoCo1.5C-700 microflower (110) surfaces are shown in this Fig.. This result demonstrated that *O adsorbed too strongly on both bare Mo_2C and MoCo1.5C-700 microflowers.





$$\Delta E_{ads} = E_{*O} - (E_* + E_{H_2O} - E_{H_2}) + \Delta ZPE - T\Delta S$$

Fig. S23 Oxygen adsorption energies for MoCo1.5C-700 microflowers (110) surfaces are shown in this Fig. . The O-covered surface was constructed by adding oxygen in increasing adsorption strength, so the last bare site (site ①) was investigated as the OER active site.

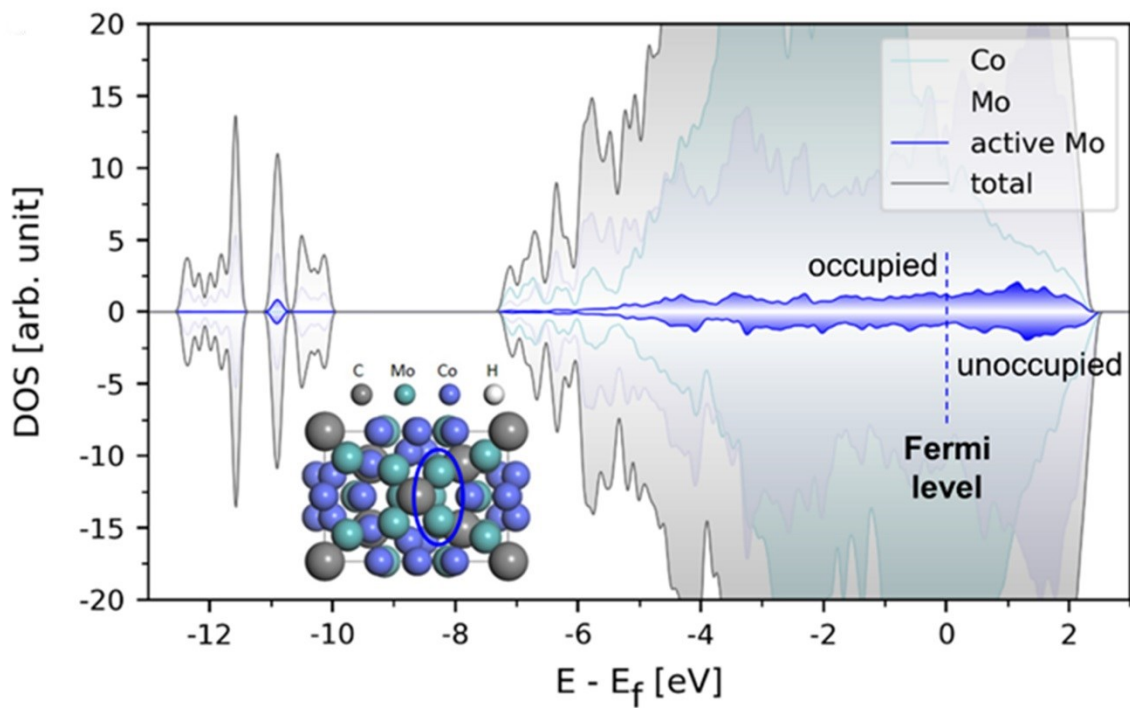


Fig. S24 Density of states (DOS) of the $\text{Mo}_3\text{Co}_3\text{C}$ (110) surface, where $E-E_f$ is energy, in which E_f is Fermi energy. The DOS of active Mo is highlighted in blue.

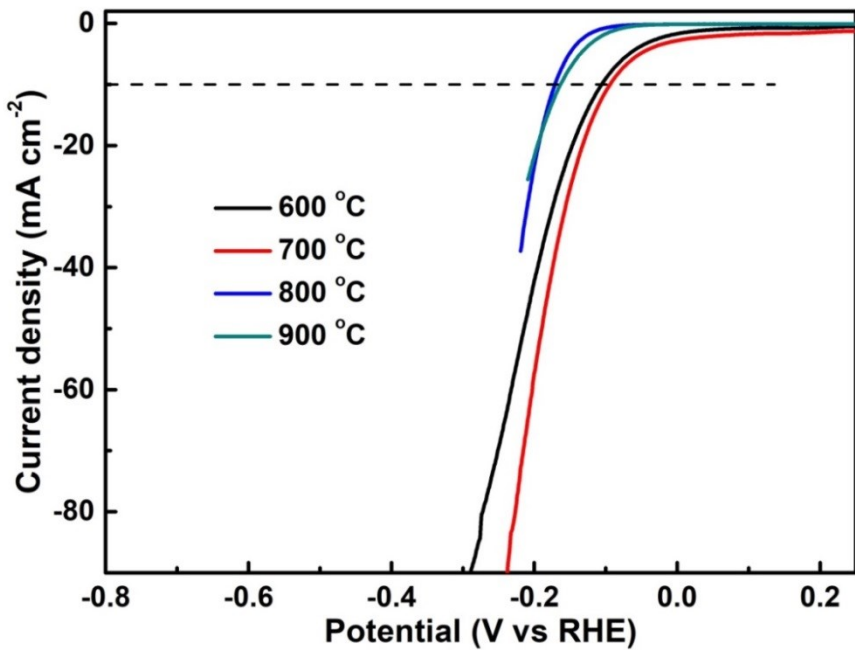


Fig. S25 HER electrocatalysis of MoCo_{1.5}C-600/700/800 microflowers and MoCo_{1.5}C-900.

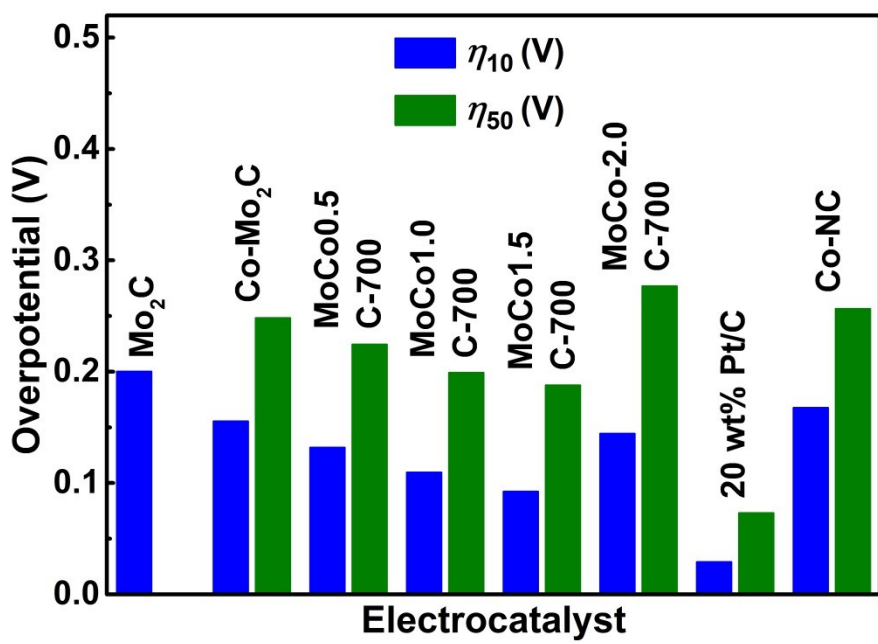


Fig. S26 HER overpotentials η_{10} and η_{50} to achieve 10 and 50 mA cm⁻² current densities, respectively, with different electrocatalysts.

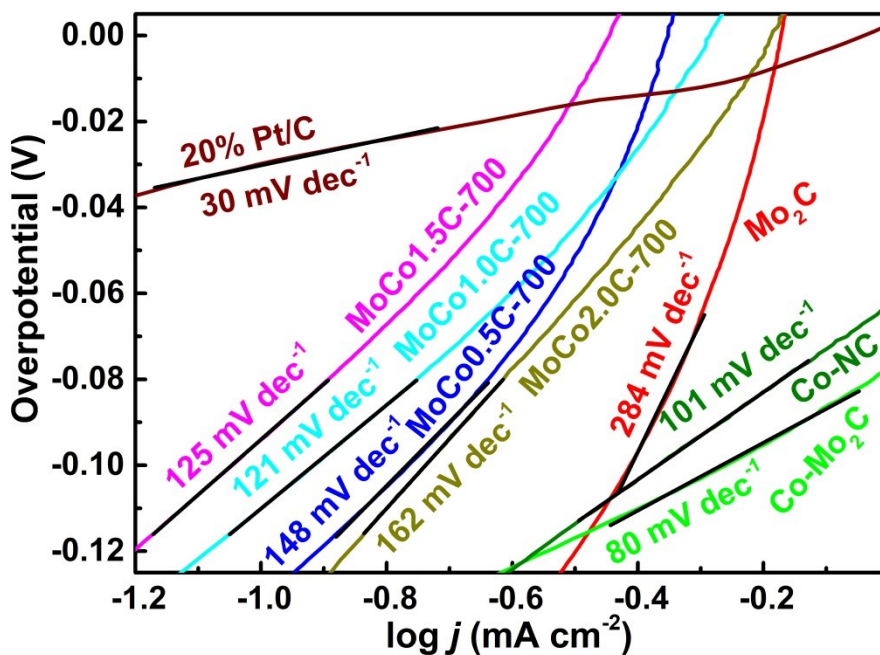


Fig. S27 Tafel slopes of different electrocatalysts for HER.

References

- 1 S. Gao, H. Chen, Y. Liu, G. D. Li, R. Gao and X. Zou, *Inorg. Chem. Front.*, 2019, **6**, 940–947.
- 2 P. Xiao, Y. Yan, X. Ge, Z. Liu, J. Y. Wang and X. Wang, *Appl. Catal. B Environ.*, 2014, **154–155**, 232–237.
- 3 J. Wan, J. Wu, X. Gao, T. Li, Z. Hu, H. Yu and L. Huang, *Adv. Funct. Mater.*, 2017, **27**, 1703933.
- 4 T. C. Xiao, A. P. E. York, H. Al-Megren, C. V. Williams, H. T. Wang and M. L. H. Green, *J. Catal.*, 2001, **202**, 100–109.
- 5 M. Li, S. Yu, Z. Chen, Z. Wang, F. Lv, B. Nan, Y. Zhu, Y. Shi, W. Wang, S. Wu, H. Liu, Y. Tang and Z. Lu, *Inorg. Chem. Front.*, 2017, **4**, 289–295.
- 6 K. Shomalian, M. M. Bagheri-Mohagheghi and M. Ardyanian, *Appl. Phys. A Mater. Sci. Process.*, 2017, **123**, 1–9.
- 7 R. Narro-García, N. Méndez, L. M. Apátiga, J. P. Flores-De los Ríos, C. G. Nava-Dino

- and R. Quintero-Torres, *Int. J. Electrochem. Sci.*, 2017, **12**, 3907–3915.
- 8 X. Zhu, X. Zhang, L. Huang, Y. Liu, H. Zhang and S. Dong, *Chem. Commun.*, 2019, **55**, 9995–9998.
- 9 J. Jiang, Q. Liu, C. Zeng and L. Ai, *J. Mater. Chem. A*, 2017, **5**, 16929–16935.
- 10 M. A. R. Anjum, M. H. Lee and J. S. Lee, *ACS Catal.*, 2018, **8**, 8296–8305.
- 11 D. Das, S. Santra and K. K. Nanda, *ACS Appl. Mater. Interfaces*, 2018, **10**, 35025–35038.
- 12 S. Wahl, S. M. El-Refaei, A. G. Buzanich, P. Amsalem, K. S. Lee, N. Koch, M. L. Doublet and N. Pinna, *Adv. Energy Mater.*, 2019, **9**, 1900328.
- 13 Y. J. Tang, C. H. Liu, W. Huang, X. L. Wang, L. Z. Dong, S. L. Li and Y. Q. Lan, *ACS Appl. Mater. Interfaces*, 2017, **9**, 16977–16985.
- 14 H. Zhang, W. Zhou, J. Dong, X. F. Lu and X. W. D. Lou, *Energy Environ. Sci.*, 2019, **12**, 3348–3355.
- 15 R. Zhang, P. A. Russo, A. G. Buzanich, T. Jeon and N. Pinna, *Adv. Funct. Mater.*, 2017, **27**, 1703158.
- 16 Q. Liang, H. Jin, Z. Wang, Y. Xiong, S. Yuan, X. Zeng, D. He and S. Mu, *Nano Energy*, 2019, **57**, 746–752.
- 17 S. Zhao, Y. Wang, J. Dong, C. T. He, H. Yin, P. An, K. Zhao, X. Zhang, C. Gao, L. Zhang, J. Lv, J. Wang, J. Zhang, A. M. Khattak, N. A. Khan, Z. Wei, J. Zhang, S. Liu, H. Zhao and Z. Tang, *Nat. Energy*, 2016, **1**, 1–10.
- 18 Q. Qian, Y. Li, Y. Liu, L. Yu and G. Zhang, *Adv. Mater.*, 2019, **31**, 1901139.
- 19 G. Hai, X. Jia, K. Zhang, X. Liu, Z. Wu and G. Wang, *Nano Energy*, 2018, **44**, 345–352.
- 20 M. J. Kim, S. Kim, D. H. Song, S. K. Oh, K. J. Chang and E. A. Cho, *Appl. Catal. B Environ.*, 2018, **227**, 340–348.
- 21 Y. Pan, K. Sun, S. Liu, X. Cao, K. Wu, W.-C. Cheong, Z. Chen, Y. Wang, Y. Li, Y. Liu,

- D. Wang, Q. Peng, C. Chen and Y. Li, *J. Am. Chem. Soc.*, 2018, **140**, 2610–2618.
- 22 Y. Huang, Q. Gong, X. Song, K. Feng, K. Nie, F. Zhao, Y. Wang, M. Zeng, J. Zhong and Y. Li, *ACS Nano*, 2016, **10**, 11337–11343.
- 23 H. Liu, J. Zhu, Z. Lai, R. Zhao and D. He, *Scr. Mater.*, 2009, **60**, 949–952.
- 24 J. R. D. S. Politi, F. Viñes, J. A. Rodriguez and F. Illas, *Phys. Chem. Chem. Phys.*, 2013, **15**, 12617–12625.
- 25 A. N. Christensen, H. Kvande, P. G. Wahlbeck and E. Näslund, *Acta Chem. Scand.*, 1977, **31a**, 509–511.
- 26 P. Li, X. Duan, Y. Kuang, Y. Li, G. Zhang, W. Liu and X. Sun, *Adv. Energy Mater.*, 2018, **8**, 1703341.